Interference and Radial Distribution Functions of Liquid Copper, Silver, Tin, and Mercury

C. N. J. WAGNER, H. OCKEN, and M. L. JOSHI

Hammond Laboratory, Yale University, New Haven, Connecticut, U.S.A.

(Z. Naturforschg. **20 a**, 325—335 [1965]; eingegangen am 21. November 1964)

The x-ray scattering from liquid copper, silver, tin, and mercury was measured at temperatures of 1125 °C, 1050 °C, 335 °C, and 28 °C, respectively, from the open surface of horizontal samples using a focusing theta-theta diffractometer, quartz crystal monochromator positioned in the diffracted beam, scintillation detector, and pulse height discriminator. The effect on the measured intensities of the positioning of the sample with respect to the diffractometer axis and the meniscus of the liquid were considered. Calibration of the primary beam intensity by measurements on liquid mercury provided an alternate check of the standard normalization procedures for copper, silver, and tin. After calculation of the interference functions, atomic and radial distribution functions were evaluated from which interatomic distances and coordination numbers were obtained. The interatomic distances in the liquid were in good agreement with the GOLDSCHMIDT diameters of the respective elements.

X-ray diffraction is one of the more important methods that may be employed to investigate the liquid state of matter. The arrangement of the atoms determines the angular distribution of the scattered x-rays. This arrangement is usually described by the probability $W(r)\,dv$ of finding the center of another atom in the volume element dv at a distance r from a given atom. Then, $W(r) = \varrho(r)/\varrho_0$, where $\varrho(r)$ is the atomic density function and ϱ_0 the average atomic density in the liquid. It can be shown that, for monatomic liquids, the radial distribution function (RDF) $4\pi r^2 \varrho(r)$ is given by [1]:

$$4\pi r^2 \varrho(r) = 4\pi r^2 \varrho_0 + (2r/\pi) \int_0^\infty K[I(K) - 1] \cdot (\sin K r)\, dK, \quad (1)$$

where $K = 2\pi s = 4\pi \sin\Theta/\lambda$, $s = 2\sin\Theta/\lambda$, and $I(K)$ is the interference function:

$$I(K) = I_{\mathrm{eu}}^{\mathrm{coh}}(K)/f^2 = I_N(K)/N f^2. \quad (2)$$

$I_N(K)$ is the coherently scattered x-ray intensity from N atoms in the irradiated volume, f the atomic scattering factor, and $I_{\mathrm{eu}}^{\mathrm{coh}} = I_N(K)/N$. The maxima in the RDF give the preferred distances of separation in the liquid; the area about these maxima gives an indication of the number of neighbors at the preferred distances.

The interference function $I(K)$ is the FOURIER transform of the radial distribution function:

$$I(K) = 1 + \int_0^\infty 4\pi r^2[\varrho(r) - \varrho_0] \cdot [(\sin K r)/K r]\, dr. \quad (3)$$

It has been shown that for large values of K, say $K > 10$ Å^{-1},

$$I(K > 10\ \text{Å}^{-1}) \sim 1 \quad (4)$$

and for $K = 0$ [1],

$$I(0) = kT\varrho_0\beta \quad (5)$$

where T is the absolute temperature, k the BOLTZMANN constant, and β the isothermal compressibility.

Since the theoretical work of ZERNIKE and PRINS [2], the diffraction patterns of many liquid metals have been measured and analyzed [3–5]. These past investigations have been primarily motivated by a desire to obtain a knowledge of preferred distances of separation and coordination numbers of nearest neighbors in the liquid state. Such information is derived from the RDF. The results reported in the literature are generally in good agreement as the RDF is quite insensitive to minor variations in the measured intensity patterns.

Recent advances in the theory of the transport properties of liquid metals [6–8] indicate that the

[1] A. GUINIER, X-Ray Diffraction in Crystals, Imperfect Crystals, and Amorphous Bodies, W. H. Freeman, San Francisco 1963.
[2] F. ZERNIKE and J. A. PRINS, Z. Phys. **41**, 184 [1927].
[3] N. S. GINGRICH, Rev. Mod. Phys. **15**, 90 [1943].
[4] K. FURUKAWA, Rep. Prog. Phys. **25**, 395 [1962].
[5] R. F. KRUH, Chem. Rev. **62**, 319 [1962].
[6] J. M. ZIMAN, Phil. Mag. **6**, 1013 [1961].
[7] C. C. BRADLEY, T. E. FABER, E. G. WILSON, and J. M. ZIMAN, Phil. Mag. **7**, 865 [1962].
[8] W. A. HARRISON, Phys. Rev. **129**, 2512 [1963].

interference function $I(K)$ plays an important role in the interpretation of these properties, particularly the electrical resistivity. To obtain accurate interference functions, it is imperative that the scattering from the liquid be accurately measured. Measurements are reported herein for liquid copper, silver, tin, and mercury. Particular attention was paid to factors affecting the measured intensities and their conversion to the interference function. The alignment procedure, correction of the relative intensity measurements for such distorting effects as polarization and absorption, contribution of the COMPTON incoherent scattering, and normalization procedures, are discussed in detail. Radial distribution and atomic distribution functions were obtained from the interference functions, and the results compared to those from previous investigations.

1. Experimental Procedure

Diffraction Geometry

The BRAGG–BRENTANO focusing geometry, in which a stationary horizontal sample is scanned by x-ray source and detector rotating in a vertical plane at equal speeds and in opposite directions, was realized with a theta-theta-diffractometer [9]. Two 12″ rotary milling tables, with an accuracy of 30 sec. of arc over the entire 360° rotation, were mounted back to face in a vertical position to drive the x-ray tube and scintillation counter. The x-ray tube was mounted with its anode end directly on the front table; the divergence slit system was attached to the tube bracket. The sample holder was rigidly mounted on the stationary front plate of the diffractometer. The standard target to specimen distance of 170 mm was used. The scintillation detector, receiving and scatter slit systems, and quartz crystal monochromator were mounted on a shaft connected to the back rotary table through the center hole of the front plate. Positioning of the monochromator in the diffracted beam eliminated the fluorescent scattering, most of the COMPTON scattering, as well as the continuous spectrum and the K_β radiation. Extraneous radiation was also eliminated by a pulse height discriminator in the detecting circuit. An electric drive mechanism for step scanning allowed the selection of steps of 0.005° to 5° in 2Θ and automatic print-out of the scattered intensity in conjunction with a transistorized timer-scaler.

The scattered x-ray intensities were measured with the fixed count technique to insure a constant statistical error ($\sim 1\%$). The x-ray intensities, measured with a system consisting of a Siemens Crystalloflex 4 generator, a Siemens Mo tube, Nuclear Picker scintillation counter, high voltage supply and printing timer-scaler, and a TMC pulse height discriminator, were found to be stable to within 1% over a period of 6 months, thus eliminating the need for monitoring of the primary beam. Measurements were made over a range of 2Θ from 10° ($K=1.5$ Å^{-1}) to 125° ($K=15.7$ Å^{-1}): at intervals of 0.5° between 10° and 80° and at intervals of 1° between 80° and 125°.

Sample Holder

A "MRC High Temperature, High Vacuum Diffractometer Attachment" [10] was modified to accommodate a crucible of 25 mm × 20 mm and to maintain temperatures in the sample up to 1200 °C [11]. The crucible size made it possible to obtain a fairly flat surface area, about 10 mm square, regardless of the surface tension of the metal under investigation. The specimen stage, together with the crucible, could be adjusted from outside the furnace by elevation and azimuthal controls so that the sample surface would be horizontal and coincident with the diffractometer axis. A pyrolytic graphite crucible was heated by radiation using a pyrolytic graphite resistance element held between two copper electrodes. A semi-circular wrought bronze heat shield with an accurately machined 10 mm wide window served to define the width of the incident and diffracted beams. A thin Al foil could be inserted in the heat shield to act as a reflector.

The furnace was flushed with an inert 90% He–10% H atmosphere during the course of the measurements to minimize oxidation of the sample surface and scattering of x-rays by the atmosphere above the sample. The power supply and temperature control system consisted of a Leeds and Northrup Speedomax Azar H recorder, CAT controller, magnetic amplifier and saturable core reactor.

The sample temperature was calibrated by measuring the freezing points of the pure metals In, Sn, Pb, Al, and Ag. The thermal arrest point of these elements was clearly detected upon cooling. An alternate calibration was provided by measuring the thermal expansion of a pure tungsten (W) powder sample (lattice parameter $a_0=3.1651$ Å). The peak shift of the highest available reflection $h^2+k^2+l^2=74$ for Mo $K_{\alpha 1}$ radiation ($\lambda=0.70926$ Å), which occurs at $2\Theta=149.11°$ at 25 °C, was measured as a function of temperature. The two calibration methods agreed to within ±10 °C. Sample temperature was maintained to within ±2 °C during the course of a measurement.

Sample Height Adjustment

Centering the primary beam about the diffractometer axis and adjusting the sample surface coincident with the diffractometer axis are the most important

[9] C. N. J. WAGNER, AEC Technical Report No. 2, Contract AT(30-1)2560.

[10] J. INTRATER and S. HURWITT, Rev. Sci. Instrum. **32**, 905 [1961].

[11] M. L. JOSHI, M. Eng. Thesis, Yale University, 1962.

requirements in the experimental set-up for the measurement of the x-ray scattering from liquids. Inaccurate centering of the primary beam upon the sample will lead to changes in intensities and positions of the low angle peaks.

After careful alignment of the theta-theta diffractometer, the peak positions of a tungsten powder sample were measured with Mo $K_{\alpha 1}$ radiation and a standard sample holder. The positions of several reflections [from (110) with $h_0^2 = h^2 + k^2 + l^2 = 2$ at $2\,\Theta_2 = 18.24°$ to (743, 750, 831) with $h_0^2 = 74$ at $2\,\Theta_{74} = 149.11°$] were measured. The coresponding lattice parameters a_{hkl} when plotted as a function of $\cos\Theta\cot\Theta$, fell on a straight, almost horizontal line, extrapolating to a value $a_0 = 3.1651$ Å at 25 °C; this agrees very well with recently published values of the lattice parameter of tungsten [12]. After placing the tungsten powder sample in the high temperature furnace, its height was adjusted so that $2\,\Theta_2 = 18.24°$ and $2\,\Theta_{74} = 149.11°$. This height, measured with a cathetometer to within ± 0.10 mm, then served as a reference for positioning of the liquid sample.

A fluorescent screen was introduced into the furnace and positioned at the correct height as determined by the above procedure. The primary beam was then centered with respect to the diffractometer axis and sample surface.

2. Analysis and Results

The interference and radial distribution functions were determined from the measured intensities with the aid of a program compiled for use with an IBM 709 computer [13]. The application of the program to the present set of measurements is described.

After subtracting the counter noise, the measured intensities I_{meas} can be related to the polarization factor P, the number of atoms N in the irradiated volume V, the coherently scattered radiation in electron units $I_{\text{eu}}^{\text{coh}}$, and the COMPTON radiation $I_{\text{eu}}^{\text{coh}}$, by the expression

$$I_{\text{meas}} \propto P\,N(I_{\text{eu}}^{\text{coh}} + I_{\text{eu}}^{\text{inc}})\,. \tag{6}$$

The number of atoms in the irradiated volume V is given by

$$N = \varrho_0\,V = Q\,\varrho_0\,A \tag{7}$$

where Q is the cross-sectional area of the primary beam of intensity I_0, ϱ_0 the average atomic density of the material, and A the absorption correction appropriate to the diffraction geometry employed in measuring the intensity scattered by the liquid. Substituting equation (7) into equation (6) and letting Φ be the constant of proportionality we obtain

$$I_{\text{meas}} = \Phi\,\varrho_0\,P\,A(I_{\text{eu}}^{\text{coh}} + I_{\text{eu}}^{\text{inc}})\,. \tag{8}$$

The measured intensity as given by the above equation must be corrected for the angular dependent factors such as absorption and polarization. If an ideally mosaic crystal is used as a monochromator, the polarization correction is

$$P = (1 + \cos^2 2\,\alpha\cos^2 2\,\Theta)/(1 + \cos^2 2\,\alpha) \tag{9}$$

where $2\,\alpha$ is the BRAGG angle of the monochromator crystal. The absorption correction for an infinitely absorbing material with a flat surface is given by

$$A = \frac{1}{\mu}\,\frac{\sin(2\,\Theta - \Delta)}{\sin\Delta + \sin(2\,\Theta - \Delta)} \tag{10}$$

where Δ is the angle between the specimen surface and the primary beam and μ is the linear absorption coefficient of the sample. When the BRAGG-BRENTANO focusing geometry is employed, $\Delta = \Theta$, and the absorption correction simplifies to $A = 1/(2\,\mu)$.

Metal	T (°C)	ϱ (gm/cm³)	Ref.	$(\mu/\varrho)\,\text{MoK}_\alpha$ [18] (cm²/gm)
Cu	1125	7.956	[14]	49.7
Ag	1050	9.24	[16]	28.6
Sn	335	6.90	[15, 16]	33.3
Hg	28	13.55	[17]	132

Table 1. Densities and mass absorption coefficients.

The corrected intensities I_{cor} are obtained by dividing the measured intensities I_{meas} by the product of the absorption and polarization corrections. The values of μ were computed from the μ/ϱ and ϱ values of Table 1. From equation (8) we obtain:

$$I_{\text{cor}} = I_{\text{meas}}/(A\,P) = \Phi\,\varrho_0(I_{\text{eu}}^{\text{coh}} + I_{\text{eu}}^{\text{inc}})\,. \tag{11}$$

[12] W. B. PEARSON, Handbook of Lattice Spacings and Structures of Metals, Pergamon Press, London 1958.
[13] H. OCKEN, Computer Applications in Metallurgical Engineering, R. D. PEHLKE and M. J. SINNOTT, editors, ASM Metals Park, Ohio 1964, p. 110.
[14] J. A. CAHILL and A. D. KIRSHENBAUM, J. Phys. Chem. **66**, 1080 [1962].
[15] K. BORNEMANN and F. SAUERWALD, Z. Metallkde. **14**, 145 [1922].
[16] I. LAUERMANN and G. METZGER, Z. Physik. Chem. **216**, 37 [1961].
[17] A. H. COOK and N. W. B. STONE, Phil. Trans. Roy. Soc. London, **250**, 729 [1957].
[18] H. S. PEISER, H. P. ROOKSBY, and A. J. C. WILSON, X-Ray Diffraction by Polycrystalline Materials, Institute of Physics, London 1955.

The corrected intensities are then normalized to the same scale as the sum of the square of the dispersion corrected atomic scattering factor and the COMPTON modified radiation. The intensity in electron units

$$I_{eu}^{coh} = \beta I_{cor} - I_{eu}^{inc} \qquad (12)$$

was obtained from equation (11) after making the substitution

$$\beta = 1/(\Phi \varrho_0) . \qquad (13)$$

The normalization constant was computed from the high-angle region method [3] and the generalized KROGH-MOE–NORMAN method [19–21].

The high-angle region method is based on the assumption that the observed corrected intensity scattered by the liquid I_{cor} converges to the total independent scattering $(f^2 + I_{eu}^{coh})$ at large scattering angles $(K > 10\ \text{Å}^{-1})$. The normalization constant can be calculated by dividing the area under the total scattering curve by the area under the corrected experimental intensity curve in the region of large K where there are no longer modulations in the latter curve. The high-angle constant β_{ha} is thus given by

$$\beta_{ha} = \int_{K\sim 10}^{K_{max}} (f^2 + I_{eu}^{inc})\, dK \Big/ \int_{K\sim 10}^{K_{max}} I_{cor}\, dK . \qquad (14)$$

The normalization constant obtained by using the KROGH-MOE–NORMAN method can be derived by considering the behavior of the expression for the RDF, equation (1), in the neighborhood of $r \sim 0$. The constant computed by this method, however, assigns a heavy weight to the intensities measured at high angles, as they are weighted by a factor of K^2. It is at large angles that the measured intensities are small, and therefore rather inaccurate. To diminish this effect, a factor of the form $\exp(-\gamma K^2)$ can be applied to the function $(I_{eu}^{coh}/f^2 - 1)$ before evaluating the KROGH-MOE–NORMAN constant [21]. The generalized KROGH-MOE–NORMAN constant β_γ is then given by

$$\beta_\gamma = \frac{\int_0^{K_{max}} (I_{eu}^{inc}/f^2 + 1)\, K^2 e^{-\gamma K^2}\, dK - 2\pi^2 \varrho_0}{\int_0^{K_{max}} (I_{cor}/f^2)\, K^2 e^{-\gamma K^2}\, dK} . \qquad (15)$$

K (Å^{-1})	Cu [22]	Ag [23]	Sn [24]	Hg [25]
0.0	866	2127	2444	6060
2.0	654	1550	1766	4700
4.0	383	900	1112	3130
6.0	216	560	685	2160
8.0	126	390	461	1540
10.0	84	298	340	1120
12.0	62	223	265	835
14.0	50	165	207	626

Table 2. Representative values of the square of the dispersion corrected (for Mo radiation) atomic scattering factors.

The quantities on the right hand side of the equations defining the high angle and generalized KROGH-MOE–NORMAN constants are either experimentally determined or obtained from the literature. Table 2 gives representative values of the dispersion corrected atomic scattering factors used in the calculations. The dispersion corrections were those of DAUBEN and TEMPLETON [26]. The values given by SAGEL [27] were used in accounting for the COMPTON incoherent scattering.

A measure of the resolving power of the quartz monochromator crystal was calculated in the following manner. After reflection from a well annealed single crystal of rocksalt, the wavelength spread of the continuous spectrum about $1/2\ \lambda$ Mo K_α ($\lambda \sim 0.35$ Å) was recorded with the monochromator positioned to reflect Mo K_α. One half of the half-width of the wavelength spread was taken as the value of $\Delta\lambda$ marking the angle at which the contribution to the COMPTON scattering had been reduced by a factor of two. The value of K at which the COMPTON radiation was resolved by the crystal was then computed from the equation $\Delta\lambda = 0.0243\,(1 - \cos 2\Theta)$. For the crystal under consideration this value of K was 7.5 Å^{-1}. The resolution of the crystal for Mo K_α should be as good as, if not better than, that for $1/2\ \lambda$ Mo K_α, since SCOTT [28] has shown that the penetration aberration is more important for shorter wavelengths.

The values of β_{ha}, $\beta_{0.0}$, and $\beta_{0.008}$, computed from equations (14) and (15), are shown in Table 3. The intensity in electron units was then obtained by multiplying the corrected intensity values by the

[19] J. KROGH-MOE, Acta Cryst. **9**, 951 [1956].
[20] N. NORMAN, Acta Cryst. **10**, 370 [1957].
[21] B. E. WARREN, private communication.
[22] A. J. FREEMAN and R. E. WATSON, Acta Cryst. **14**, 231 [1961].
[23] M. L. POTTERS, unpublished. (see International Tables for X-Ray Crystallography, Vol. III, Kynoch Press, Birmingham, England, 1962)
[24] A. J. FREEMAN and R. E. WATSON, private communication.
[25] J. A. IBERS, Acta Cryst. **11**, 447 [1958].
[26] C. H. DAUBEN and H. TEMPLETON, Acta Cryst. **8**, 841 [1955].
[27] K. SAGEL Tabellen zur Röntgenstrukturanalyse, Springer-Verlag, Berlin 1958.
[28] R. E. SCOTT, Rev. Sci. Instrum. **35**, 118 [1964].

Metal	high angle method β_{ha} ($\times 10^{-4}$)	Krogh-Moe–Norman method β_0 ($\times 10^{-4}$)	Krogh-Moe–Norman method $\beta_{+0.008}$ ($\times 10^{-4}$)	average value ($\times 10^{-4}$)	diffraction geometry constant ($\times 10^{-4}$) (Hg standard)
Cu	1.88	1.91	1.93	1.91	1.94
Ag	2.78	2.78	2.79	2.78	2.84
Sn	3.86	3.96	4.04	3.95	4.18
Hg	3.58	3.58	3.63	3.60	3.60

Table 3. Values of the normalization constant β: $I_{eu}^{coh}=\beta I_{cor}-I_{eu}^{inc}$.

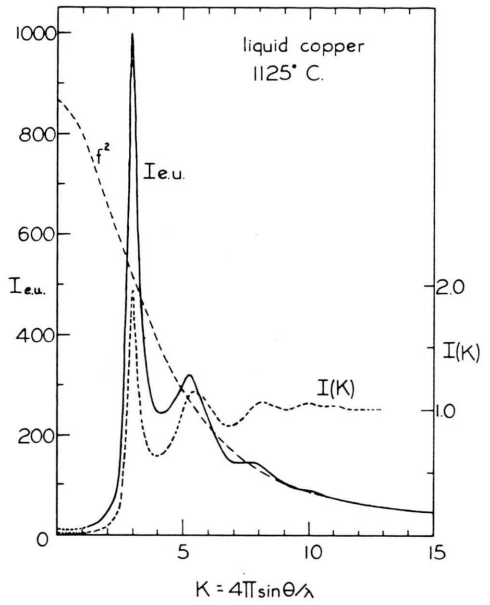

Fig. 1. The absolute intensity function I_{eu} and interference function $I(K)$ of liquid copper at 1125 °C.

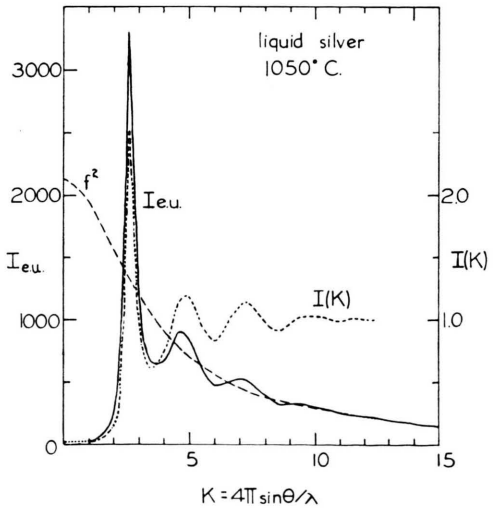

Fig. 2. The absolute intensity function I_{eu} and interference function $I(K)$ of liquid silver at 1050 °C.

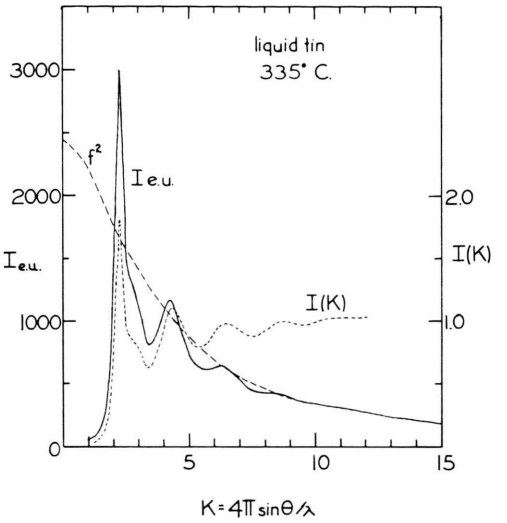

Fig. 3. The absolute intensity function I_{eu} and interference function $I(K)$ of liquid tin at 335 °C.

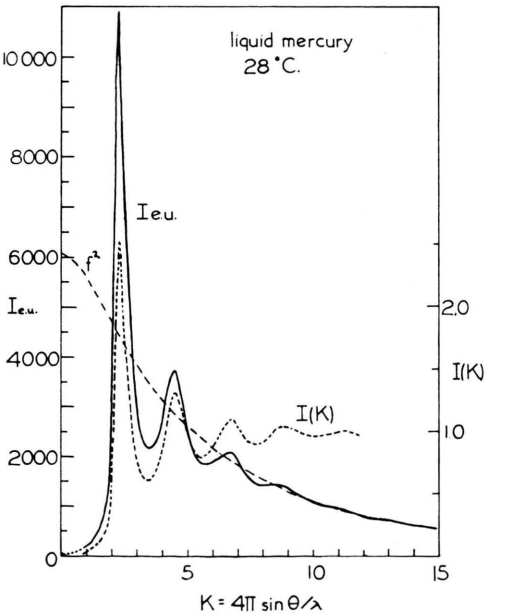

Fig. 4. The absolute intensity function I_{eu} and interference function $I(K)$ of liquid mercury at 28 °C.

	Cu	Ag	Sn	Hg
T (°C)	1125	1050	335	28
K (Å^{-1})	$I(K) = I_{eu}^{coh}/f^2$			
1.6	0.03	0.05	0.10	0.13
1.7	0.04	0.07	0.15	0.18
1.8	0.05	0.09	0.23	0.23
1.9	0.06	0.13	0.40	0.34
2.0	0.07	0.17	0.71	0.60
2.1	0.09	0.28	1.20	1.19
2.2	0.11	0.45	1.50	1.93
2.3	0.14	0.73	1.61	2.40
2.4	0.19	1.21	1.37	2.03
2.5	0.32	1.81	1.02	1.76
2.6	0.48	2.28	0.91	1.51
2.7	0.70	2.08	0.87	1.31
2.8	1.18	1.70	0.84	1.11
2.9	1.70	1.14	0.82	0.93
3.0	1.77	1.00	0.78	0.79
3.1	1.44	0.84	0.75	0.71
3.2	1.20	0.72	0.70	0.65
3.3	1.00	0.67	0.65	0.63
3.4	0.86	0.63	0.63	0.61
3.5	0.77	0.62	0.65	0.62
3.6	0.70	0.63	0.69	0.63
3.7	0.66	0.65	0.74	0.67
3.8	0.64	0.67	0.80	0.71
3.9	0.62	0.70	0.87	0.79
4.0	0.62	0.74	0.94	0.86
4.2	0.65	0.89	1.08	1.06
4.4	0.70	1.03	1.08	1.27
4.6	0.79	1.16	1.01	1.29
4.8	0.90	1.19	0.94	1.16
5.0	1.02	1.19	0.81	0.98
5.2	1.13	1.11	0.81	0.85
5.4	1.15	0.99	0.80	0.79
5.6	1.13	0.92	0.81	0.79
5.8	1.08	0.88	0.85	0.83
6.0	1.03	0.83	0.91	0.88
6.2	0.97	0.87	0.97	0.94
6.4	0.92	0.93	0.98	1.01
6.6	0.87	1.01	0.98	1.07
6.8	0.87	1.07	0.96	1.10
7.0	0.86	1.12	0.93	1.05
7.2	0.90	1.15	0.90	0.97
7.4	0.95	1.13	0.88	0.92
7.6	1.00	1.09	0.87	0.90
7.8	1.03	1.04	0.89	0.90
8.0	1.06	0.98	0.93	0.91
8.2	1.06	0.94	0.96	0.95
8.4	1.02	0.92	0.98	0.99
8.6	1.03	0.91	1.00	1.03
8.8	1.01	0.94	1.01	1.04
9.0	1.02	0.98	1.00	1.04
9.2	1.00	1.01	0.98	1.02
9.4	1.01	1.01	0.97	0.99
9.6	1.03	1.03	0.98	0.97
9.8	1.05	1.02	0.98	0.97
10.0	1.06	1.03	1.00	0.97
10.2	1.04	1.01	1.01	0.97
10.4	1.04	1.02	1.02	0.98
10.6	1.03	1.01	1.03	0.99
10.8	1.02	1.00	1.03	1.00
11.0	1.03	1.00	1.03	1.01
11.2	1.02	1.00	1.03	1.01
11.4	1.01	1.02	1.03	0.99
11.6	1.00	1.01	1.02	0.98
11.8	1.00	1.00	1.02	0.97
12.0	1.01	1.01	1.03	0.95

Table 4. The interference functions of liquid copper, silver, tin, and mercury.

average of the three normalization constants. The absolute intensities I_{eu}^{coh} and interference functions $I(K)$ are shown in Figs. 1, 2, 3, and 4 for copper, silver, tin, and mercury, respectively. The values of $I(K)$ are listed in Table 4.

The function $K[I(K)-1]$, hereafter referred to as $Ki(K)$, can then be generated from the interference function. At low values of K, where data was unavailable, a linear interpolation was assumed between $K=0$ and $K=1.5$ Å^{-1}. Prior to the FOURIER transformation, $Ki(K)$ was terminated at $K=12.0$ Å^{-1} and weighted by the factor $\exp(-0.005\,K^2)$. Radial distribution functions so calculated are shown in Figs. 5 through 8. Similar transformations were calculated for $Ki(K)$ terminated at the following values of K_{max} and weighted by factors of the form $\exp(-\sigma K^2)$: $K_{max}=12.0$ Å^{-1} and $\sigma=0$, $K_{max}=7.5$ Å^{-1} and $\sigma=0$. The latter value of K_{max} represents the approximate upper limit to which the x-ray scattering from liquids can be measured if Cu K_α radiation is used.

Distances of closest approach were obtained from these curves by extrapolating the midpoints of the peak to the peak maximum. The interatomic distances, obtained from the atomic distribution function $W(r)$ after inversion of $Ki(K)$ terminated at $K=12.0$ Å^{-1}

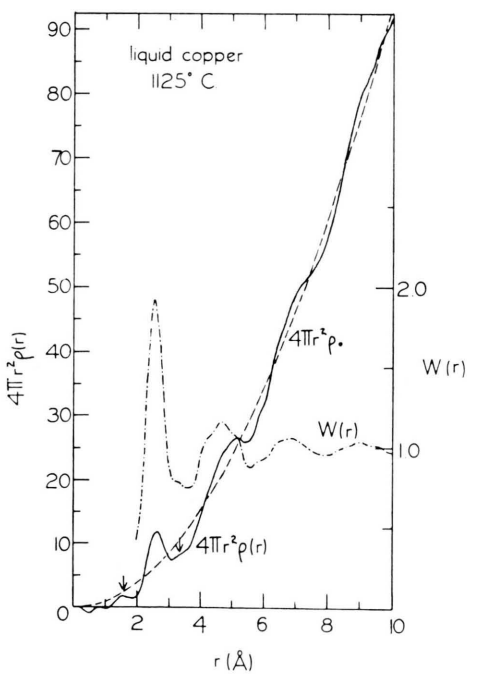

Fig. 5. The radial distribution function $4\pi r^2 \varrho(r)$ and probability function $W(r)$ of liquid copper at 1125 °C.

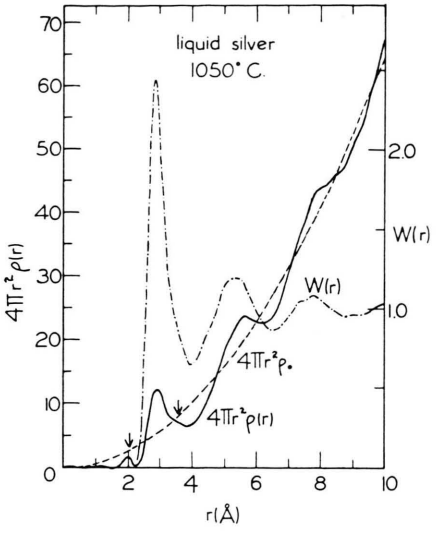

Fig. 6. The radial distribution function $4\pi r^2 \varrho(r)$ and probability function $W(r)$ of liquid silver at 1050 °C.

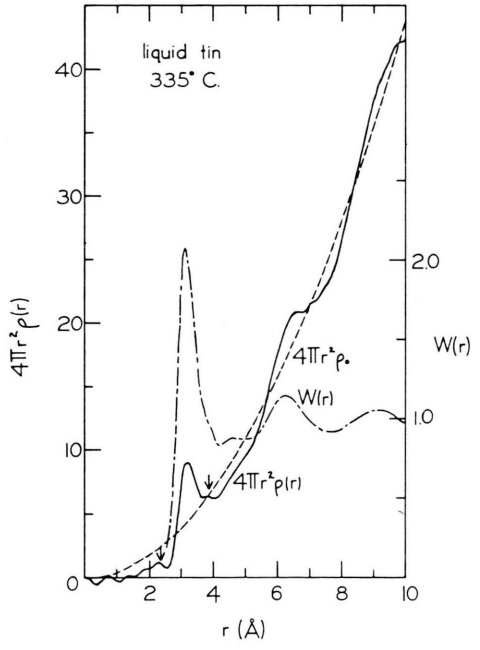

Fig. 7. The radial distribution function $4\pi r^2 \varrho(r)$ and probability function $W(r)$ of liquid tin at 335 °C.

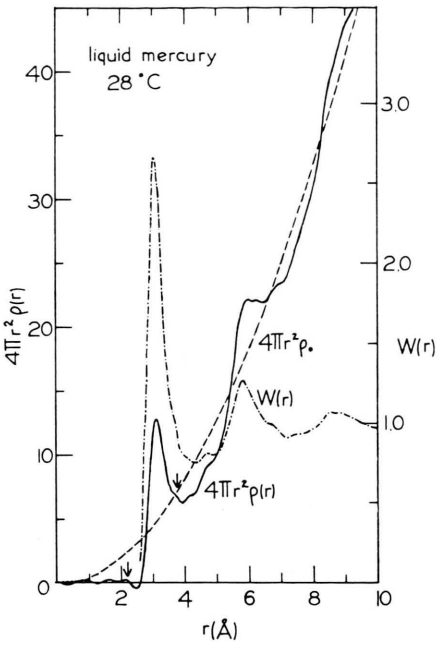

Fig. 8. The radial distribution function $4\pi r^2 \varrho(r)$ and probability function $W(r)$ of liquid mercury at 28 °C.

and weighted by the factor $\exp(-0.005\,K^2)$, were 2.55 Å for copper at 1125 °C, 2.84 Å for silver at 1050 °C, 3.14 Å for tin at 335 °C, and 3.05 Å for mercury at 28 °C. Coordination numbers were obtained by integrating the first peak of the RDF from $r=0$ to $r=r_0$, r_0 being the minimum value of the RDF after the first maximum. The values obtained were 11.5 atoms for copper and silver, 8.5 atoms for tin, and 10.0 atoms for mercury. The results of the FOURIER analyses are summarized in Table 5.

3. Discussion

Measured Intensity Data

The analysis presented above is predicated on the assumption that the following experimental conditions are satisfied:

	T (°C)	RDF r_1 (Å)			$W(r)$ r_1 (Å)			GOLDSCHMIDT diameter (Å)	CN
		$K=12.0$ $\sigma=0$	7.5 0	12.0 +0.005	12.0 0	7.5 0	12.0 +0.005		
Cu	1125	2.60	2.62	2.61	2.55	2.55	2.55	2.551	11.5
Ag	1050	2.85	2.96	2.87	2.83	2.88	2.84	2.883	11.5
Sn	335	3.17	3.29	3.20	3.13	3.22	3.14	3.164	8.5
Hg	28	3.07	3.14	3.09	3.05	3.07	3.05	3.10	10.0

Table 5. Values of the interatomic distance r_1 obtained from the radial distribution function RDF and the probability function $W(r)$. The GOLDSCHMIDT atomic diameters and the measured coordination numbers are also included.

(1) The relative scattered intensity is measured over a wide range of the scattering angle 2Θ.

(2) Monochromatic radiation of uniform intensity is used.

(3) The sample is accurately positioned with respect to the primary beam and the diffractometer axis.

The degree to which the experimental methods described in the preceeding sections meet these requirements will now be considered.

The use of Mo K_{α_2} radiation insures that the scattered intensity is measured over a sufficiently large value of K; at 2Θ equal to 125°, K is equal to 15.7 $Å^{-1}$. For measurements beyond K approximately 12 $Å^{-1}$, it is observed that I_{eu}^{coh} is nearly equal to f^2.

The characteristic radiation was isolated by reflecting the diffracted beam from a ground and bent quartz single crystal. Although it was possible to eliminate most of the K_{α_2} component, this was not done to avoid reducing further the already weak intensities scattered by the liquid sample. The pulse height discriminator served to eliminate the $\lambda/2$ wavelength reflected by the quartz crystal.

The absorption correction defined by equation (10) assumes that the irradiated area of the sample is flat. The primary beam of limited divergence striking the meniscus of the sample has the effect, however, of introducing a variable angle of incidence (Fig. 9). This angle varies from $(\Theta_0+\varepsilon_m)$ to $(\Theta_0-\varepsilon_m)$; Θ_0 is the nominal value of the angle of incidence and ε is the angle between the horizontal plane and the tangent to the surface of the specimen. For the metals under investigation, which do not wet the crucible, the meniscus is convex, and ε is positive. A variable angle of incidence would lead to an angular dependent correction factor even if the focusing geometry were used. When the angle of incidence is $(\Theta_0\pm\varepsilon)$, the absorption correction becomes

$$A=\frac{1}{2\mu}(1\mp\tan\varepsilon\cot\Theta_0). \tag{16}$$

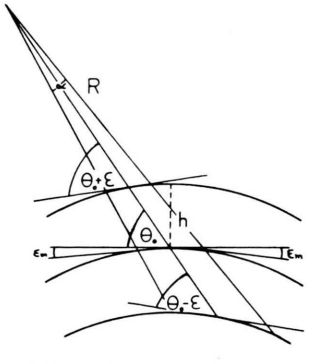

Fig. 9. Change of the angle of incidence with sample curvature and sample displacement.

If the primary beam is centered upon the sample surface, it is reasonable to assume that the terms in the above correction factor are small when averaged from $+\varepsilon_m$ to $-\varepsilon_m$, and the standard absorption correction is applicable.

If a flat portion of a sample, positioned above or below the diffractometer axis, is symmetrically irradiated by the primary beam, the only effect should be a displacement ΔK of the diffraction positions 2Θ:

$$\Delta K=\frac{4\pi}{\lambda}\frac{h}{R}\cos^2\Theta \tag{17}$$

where h is the displacement of the sample from the diffractometer axis, R is the radius of the diffractometer and λ is the wavelength of the x-rays. The diffracted intensities should remain unchanged.

Measurements of the first two maxima from samples of liquid Hg, which were positioned to either side of the diffractometer axis, indicated, however, changes both in peak positions and peak intensities. Positioning the sample below the diffractometer axis shifted the peak maxima to lower angles and resulted in higher diffracted intensities. Conversely, a sample positioned above the diffractometer axis gave rise to peak maxima displaced to higher angles and weaker diffracted intensities. If the primary beam is centered upon the diffractometer axis, positioning the sample above the axis will cause the beam to strike the sample at a point to the left of center (Fig. 9). This is equivalent to an angle of incidence greater than the nominal value Θ_0, and ε is therefore positive. A similar argument leads to the conclusion that positioning the sample below the diffractometer axis gives rise to a negative value of ε. The change in diffracted intensities resulting from a change in position of the sample with respect to the diffractometer axis is then consonant with equation (16). The change in the scattered intensity of the first peak of liquid mercury was about $\pm 6\%$ for a sample positioned ∓ 0.15 mm to either side of the diffractometer axis.

For accurate measurement of the intensities scattered by a liquid it is therefore imperative that the sample be properly positioned with respect to the diffractometer axis and be symmetrically irradiated

by the primary beam. The two correction factors are more important for measurements at low angles, because both cot Θ [equation (16)] and $\cos^2\Theta$ [equation (17)] decrease as Θ increases.

The effect of different alignment procedures on the relative scattered intensity values was provided by a comparison with earlier measurements on liquid tin [11] and mercury [13]. The non-focusing diffraction geometry, with an angle of incidence of the primary beam of $\Delta = 5.5$, was achieved by affixing the sample holder to a Norelco dliffractometer. The use of balanced filters rather than a quartz monochromator for isolation of Mo K_α marked the only difference in the experimental arrangements. The specimen alignment procedure, however, was that described by FURUKAWA [4]. Consequently, the apparatus was set for the maximum peak position and further adjustment of the liquid level was made until the strongest scattered intensity was obtained. In contrast to the alignment procedure previously described, FURUKAWA's procedure would lead to a sample positioned below the diffractometer axis. According to the above analysis of the effect of sample position on scattered intensities, larger scattered intensities should be measured. Such, indeed, was found to be the case. The measured intensities I_{meas} of the first peak for both liquid tin and mercury were about 25% higher for non-focusing diffraction geometry data, as compared to focusing diffraction geometry data.

Absolute Intensity Data and Interference Functions

While the discrepancy between the high angle and generalized KROGH-MOE–NORMAN method normalization constants has been found to be small (on the order of 3% with the exception of tin), this agreement does not give any indication of the accuracy of the measurements from the different materials. A normalization procedure has been used by the authors which enables one to establish the accuracy of the overall measurements. The method allows the calibration of the primary beam intensity from the measured intensities scattered by a reference liquid.

From equation (13) the normalization constant was found to be $\beta = 1/(\Phi\,\varrho_0)$. Φ is a factor which measures the scattering power of each atom and has dimensions of Å^2/atom. For a given diffraction arrangement, Φ is independent of the material under investigation. Once its value has been determined, it can be used as the normalization factor for all other measurements.

Since Φ depends critically on β (the normalization constant), the following criteria should be met by the material chosen as the reference liquid. The scattering factor should be accurately known. The surface tension should be small so that the curvature of the sample surface is minimal; the standard absorption correction can then be applied with assurance. The scattering power of the material should be large in order to minimize excessively long counting periods in the measurement of the scattered intensities. These requirements are amply fulfilled by liquid mercury. In addition, its being liquid at room temperature eliminates the necessity for any high temperature diffractometer furnace. The diffraction geometry normalization factor obtained for mercury was $\Phi = 6.83 \times 10^{-4}$ Å^2/atom. Using this value, the normalization constants were then computed for the other elements under investigation. These values are given in Table 3 together with the values obtained using the standard normalization methods. The values determined from the diffraction geometry factor can be viewed as the predicted values of the normalization constants; the values in the other columns represent experimentally determined values.

The large discrepancy in the value obtained for liquid tin is most probably due to errors in the f^2 values. The most recent determination of f for tin [24] differs by as much as $\pm 4\%$, at large values of K, from older values [29–31]. It is of interest to note that if the normalization constant computed from the diffraction geometry normalization factor is used to normalize the tin data, the resulting absolute intensity values fall within the spread of the various tabulated f^2 values at high angles.

A further indication of the accuracy of the alignment procedure and normalization methods was obtained from the scattering of liquid copper at low angles. The first maximum in the intensity curve is at a relatively large value of K (3.00 Å^{-1}) so that the scattering from the low angle side of this peak can be measured. The measured scattering from $K = 1.6$ Å^{-1} to $K = 2.4$ Å^{-1} was approximately constant and could be safely extrapolated to $K = 0$.

[29] L. PAULING and J. SHERMAN, Z. Krist. A **81**, 1 [1932].
[30] L. H. THOMAS and K. UMEDA, J. Chem. Phys. **26**, 239 [1957].
[31] R. W. JAMES and G. W. BRINKLEY, Phil. Mag. **12**, 81 [1931].

Using equation (5), a value of 0.95×10^{-12} cm²/dyne was calculated as the isothermal compressibility of liquid copper. Extrapolating values of the isothermal compressibility of solid copper to the melting point [32] and assuming a 10% increase in this value upon melting yields a value of 1.04×10^{-12} cm²/dyne.

An exacting measure of the accuracy of studies of the x-ray scattering from liquids is provided by a comparison of the magnitudes of the first peak of the interference function. It is at low angles that improper positioning of the sample will result in significant variations in the measured intensities and, consequently, the interference function. The magnitude of the first maximum of $I(K)$ of past and present studies of liquid copper, silver, tin, and mercury are given in Table 6. The agreement in most cases is poor. It is unlikely that the temperature dependence of the x-ray scattering can account for such significant differences. Only in the case of measurements on liquid mercury using diffractometer techniques is there any measure of consistency. Here, however, the intensities measured by KRUH, et al. [40] are lower than those obtained by PFANNENSCHMID [34], KAPLOW and AVERBACH [41], and the present workers. The values of $I(K_1)$ reported here for silver and tin are smaller than those previously reported in the literature. The discrepancies are certainly due to different alignment procedures used in positioning the liquid sample with respect to the diffractometer axis and the primary beam. If accurate measurements are to be made of the x-ray scattering from liquids, close attention must be paid to accurate positioning of the specimen.

The Radial Distribution Function

Inaccurate x-ray intensity measurements and those over a small range of K lead to errors in the RDF. Such errors generally appear as spurious ripples or subsidiary maxima. The spurious ripples can arise from a large error in the measured intensity pattern at a discrete angular position [42] or from using an

metal	T (°C)	ref.	diffraction geometry	radiation	monochromator	detector	I_{eu} K_1 (Å^{-1})	$I(K_1)$	RDF r_1 (Å)	K_{max} (Å^{-1})
Cu	1090	[33]	B. B.	Cu	C	G. M.	–	—	2.57	—
	1125	present work	B. B.	Mo	C	S. C.	2.96	1.95	2.61	12.0
Ag	1000	[34]	N. F.	Mo	C	P. C.	2.62	2.75 *	2.86	13.7
	1050	present work	B. B.	Mo	C	S. C.	2.62	2.50	2.87	12.0
Sn	250	[35]	N. F.	Mo	C	F.	2.18	2.10 *	3.38	—
	280	[36]	N. F.	Mo	C	F.	2.20	2.30 *	3.20	9.2
	232	[37]	B. B.	Cu	C	G. M.	2.24	2.00 *	3.27	7.3
	335	present work	B. B.	Mo	C	S. C.	2.26	1.80	3.20	12.0
									3.29	7.5
Hg	18	[38]	N. F.	Cu, Ag	C	F.	2.29	2.00 *	3.00	12.0
	—	[34]	N. F.	Mo	C	P. C.	2.28	2.35 *	3.05	13.7
	23	[39]	B. B.	Mo	C	S. C.	2.30	—	3.06	—
	26	[40]	B. B.	Mo	C	S. C.	2.35	~1.85 *	3.03	12.0
	21	[41]	B. B.	Cr, Co, Mo	C	S. C.	2.35	2.50	—	—
	28	present work	B. B.	Mo	C	S. C.	2.27	2.50	3.09	12.0

Table 6. Summary of x-ray studies of liquid copper, silver, tin, and mercury.
B. B., BRAGG-BRENTANO focusing geometry; N. F., non-focusing diffraction geometry; C, crystal monochromator; G. M., GEIGER-MÜLLER counter; S. C., scintillation counter; P. C., proportional counter; F., film. — * Taken from I_{eu} and converted into $I(K_1)$.

[32] H. B. CALLEN, Thermodynamics, John Wiley & Sons, New York 1960.
[33] B. R. ORTON and G. I. WILLIAMS, unpublished, see ref. [37].
[34] O. PFANNENSCHMID, Z. Naturforschg. **15a**, 603 [1960].
[35] C. GAMERTSFELDER, J. Chem. Phys. **9**, 450 [1941].
[36] H. HENDUS, Z. Naturforschg. **2a**, 505 [1947].
[37] K. FURUKAWA, B. R. ORTON, J. HAMOR, and G. I. WILLIAMS, Phil. Mag. **8**, 141 [1963].
[38] H. HENDUS, Z. Naturforschg. **3a**, 416 [1948].
[39] Y. S. KIM, C. L. STANDLEY, R. F. KRUH, and G. T. CLAYTON, J. Chem. Phys. **34**, 1464 [1961].
[40] R. F. KRUH, G. T. CLAYTON, C. HEAD, and G. SANDLIN, Phys. Rev. **129**, 1479 [1963].
[41] R. KAPLOW and B. L. AVERBACH, Rev. Sci. Instrum. **34**, 579 [1963].
[42] H. P. KLUG and L. E. ALEXANDER, X-Ray Diffraction Procedures, John Wiley & Sons, New York 1954.

incorrect value for the normalization constant [43]. The subsidiary maxima on either side of a main peak result from terminating the FOURIER series at a finite value of K [44].

Subsidiary maxima arising from the termination error are relatively easy to trace as their position is a function of the upper limit of integration. They appear at $\Delta r = \pm 5\,\pi/2\,K_{max} = \pm 7.85/K_{max}$ according to the analysis of SUGUWARA [45] or at

$$\Delta r = \pm 8\,\pi/3\,K_{max} = \pm 8.36/K_{max}$$

according to the analysis of BRAGG and WEST [46] from the main peak positions. Shifts in RDF peak positions obtained from data terminated at the two different values of K enabled one to ascertain those peaks arising from the termination error. These peaks are marked with an arrow in Figs. 5 through 8.

The effect of decreasing the information in $K\,i(K)$ either by applying a weighting factor or by terminating the curve at a smaller value of K is to shift the position of the peak maxima in the radial distribution [40] and $W(r)$ functions to larger values of r. The shift is smaller when a damping factor is applied as compared to when the curve is terminated at a smaller value of K. A striking illustration of the effect of terminating the measurements at too low an angle occurs in the case of liquid tin. Terminating the data at $K = 12.0$ Å^{-1} yielded a RDF with $r_1 = 3.18$ Å. Terminating the same data at $K = 7.5$ Å^{-1} gave a RDF with $r_1 = 3.29$ Å. This latter value is in excellent agreement with that of FURUKAWA et al., who, measuring the scattering from liquid tin with Cu K_α radiation and terminating the FOURIER transformation at $K_{max} = 7.3$ Å^{-1} obtained a value $r_1 = 3.27$ Å. The advantage of applying a damping factor to $K\,i(K)$ is that it serves to reduce the magnitude of the subsidiary maxima [44]. The values of the damping factor constant $\sigma = 0.005$ and $K_{max} = 12.0$ Å^{-1} used to obtain the radial distribution functions of Figs. 5 through 8 gave results almost free of ripples with little change in r_1 due to loss of information in $K\,i(K)$.

Distances of closest approach obtained from past and present studies are summarized in Table 6. In most cases, these values are in good agreement even though the measured intensity patterns may be significantly different. The insensitivity of the main features of the RDF to the details of the interference function is due to the fact that the interference function is weighted by K prior to the FOURIER transformation. The data at small K, which are most sensitive to misalignment of the sample, therefore do not play an excessive role in the integral. As noted previously, errors in the intensity measurements at large K, arising from a poor signal to noise ratio, are prevented from assuming a disproportionate role in the integration by application of a suitable weighting factor. Differences in the distance of closest approach may also result from the use of different values of f^2 in the analysis of the data and from the use of different upper limits of integration.

The values of the interatomic distances r_1, obtained from the probability functions $W(r)$, can be compared to the GOLDSCHMIDT diameters [47] of the corresponding metals. These diameters, the distances of closest approach for a coordination number of twelve, are also given in Table 5. The values agree to within 3%. The agreement between the two figures for each element would be somewhat improved if the small decrease in the GOLDSCHMIDT atomic diameter with decreasing coordination number were taken into account. For elements crystallizing in close packed structures in the solid state, viz., copper and silver, there is virtually no change in interatomic spacing during the solid-liquid transition. The values of the interatomic spacing and the increase in coordination number for mercury and tin indicate that the open-packed structures of the solid state break down and become closer to an ideal monatomic structure, characteristic of a metal, in the liquid state.

Acknowledgments

The authors wish to thank Drs. N. E. CUSACK and A. PASKIN for their comments on the manuscript, particularly for suggesting the format of Table 4. The financial support of the Atomic Energy Commission through contract SAR/AT(30-1)2560 is gratefully acknowledged.

[43] A. BIENENSTOCK, J. Chem. Phys. **31**, 570 [1959].
[44] C. FINBAK, Acta Chem. Scand. **3**, 1279, 1293 [1949].
[45] T. SUGAWARA, Sci. Rep. Res. Inst. Tohoku Univ. Ser. A **3**, 39 [1951].
[46] W. L. BRAGG and J. WEST, Phil. Mag. **10**, 823 [1930].
[47] W. HUME-ROTHERY, Structure of Metals and Alloys, Institute of Metals, London 1945.